Catalysis Science & Technology

Accepted Manuscript

ROYAL SOCIETY OF CHEMISTRY

rsc.li/catalysis

View Article Online
DOI: 10.1039/C9CY00130A

Catalysis Science & Technology

ARTICLE

PrOx catalysts for the combustion of soot generated in diesel engines. Effect of CuO and 3DOM structure

Received 00th January 20xx,
Accepted 00th January 20xx

DOI: 10.1039/x0xx00000x

www.rsc.org/

Virginia Alcalde-Santiago, Esther Bailón-García*, Arantxa Davó-Quiñonero, Dolores Lozano-Castelló, Agustín Bueno-López

PrO_x and CuO/PrO_x catalysts have been prepared with conventional (Ref) and three dimensionally order macroporous (3DOM) structures, and the effect of the structure on the soot combustion has been studied. It has been demonstrated that the 3DOM structure significantly improves the catalytic combustion of soot with O_2. The activity follows the trend PrO_x-3DOM > CuO/PrO_x-3DOM ~ CuO/PrO_x-Ref >> PrO_x-Ref, which is explained considering two aspects: the production of active oxygen and its transfer from catalyst to soot. FESEM microscopy, N_2 adsorption, Hg porosimetry and He density show that the 3DOM catalysts have ordered macroporosity with pores of 80 nm in diameter, which favors the carbon-catalyst contact. In addition, 3DOM catalysts present higher surface density of active oxygen (O_{ads}), which follows the trend CuO/PrO_x-3DOM > PrO_x-3DOM ~ CuO/PrO_x-Ref > PrO_x-Ref. Consequently, the PrO_x-3DOM catalyst combines a good production of active oxygen and an efficient transfer to soot, being the most active catalyst to accelerate soot combustion. On the contrary, PrO_x-Ref is the least active since it is the least efficient producing and transferring active oxygen. The impregnation of copper on the conventional support (CuO/PrO_x-Ref) enhances the production and transfer of active oxygen, improving the activity with respect to PrO_x-Ref. However, CuO blocks the porosity of the 3DOM support, hindering the contact with soot. Soot combustion is accelerated in the presence of NO_x due to the production of NO_2. This NO_2, once produced, is mostly readsorbed on the surface of the catalysts producing active oxygen that must be transferred to soot. For this reason, the porosity of the catalysts also plays a relevant role during combustion with NO_x/O_2 because affects the transfer of active oxygen produced by NO_2 to soot.

Department of Inorganic Chemistry. University of Alicante. Carretera de San Vicente s/n. E03080, Alicante (Spain). E-mail: estherbg@ugr.es

View Article Online
DOI: 10.1039/C9CY00130A

Introduction

Air pollution generated by mobile sources is a problem of general interest that the today's society must face.[1] Among the pollutants present in the exhaust gases of diesel engines, soot and NOx are those which present the greatest challenge in terms of their control and elimination.[2]

Diesel particles spontaneously burn in air at about 500–600 ^{o}C,[3] nevertheless, the temperature of the exhaust gases of modern diesel engines is relatively low (150–500 ^{o}C)[4] and therefore, a catalyst is needed to increase the oxidation rate at low temperatures. It has been proved that ceria is an excellent catalyst to accelerate soot combustion due to its high availability of surface oxygen, the ability of cerium cations to change its oxidation state during the reaction and, hence, its capacity to exchange oxygen with the gas phase.[5] During this oxygen exchange highly reactive oxygen radicals are created, usually referred to as “active oxygen”, which are highly oxidizing and very efficient for soot combustion.[6] The formation of this "active oxygen" is further enhanced by the addition of small amounts of metal, for example Cu, which improves the oxygen exchange between ceria and O_2.[7] Nevertheless, the reaction between “active oxygen” and soot is limited by the solid-solid contact.

In addition, the soot combustion is enhanced in presence of NO_x, which is present in the exhaust gases of diesel engines, by the so-called “NO_2-assisted mechanism”.[6] NO_2 is more oxidizing than NO and O_2 and so, in presence of NO_2 the combustion begins to occur already at 250 ^{o}C.[8] Nevertheless, NO_x emissions from diesel engines are typically composed of NO (only 5% of the total NO_x emissions is NO_2),[6] and to enhance the soot combustion by this mechanism, NO has to be oxidized to NO_2. In this sense, ceria catalyzes the oxidation of NO to NO_2 and this NO_2 i) could directly react with soot improving the soot combustion due to the better gas-solid contact in comparison with the solid-solid one needed for the active oxygen mechanism or ii) could be adsorbed on ceria generating more active oxygen by the decomposition of nitrogen-containing groups and consequently, contributes to a greater extent to soot oxidation.[9]

Active oxygen is more oxidant than NO_2 and, therefore, it is desirable to enhance this contribution. To really increase the effectiveness of the active oxygen combustion, either created by O_2 or by NO_2, a good solid-solid contact between soot and catalyst is required.[10] In this sense, the use of catalysts with three-dimensional ordered macroporous structure (3DOM) greatly improves the soot combustion due to the improvement of such solid-solid contact.[10–12]

Akin to ceria, praseodymia can adopt oxygen-deficient stoichiometries, and even, the Pr^{4+}/Pr^{3+} pair has a greater reduction potential than the Ce^{4+}/Ce^{3+} pair. It has been previously demonstrated that PrO_{2-x} provides a good response in the soot combustion at low temperatures in presence of O_2,[13] even slightly better than Zr-doped ceria catalysts, probably because of the ease reducibility of the Pr^{4+} cations on the surface compared to Ce^{4+}. These Pr^{3+} cations are responsible for the activation of oxygen on the surface, probing that praseodymia participates actively in the active oxygen-assisted soot combustion.[13] In addition, in the presence of NO, praseodymia presents an important ability for the NO_2 production,[13] greater than ceria, which accelerates to a greater degree the combustion of soot through the NO_2-assisted mechanism.

In spite of the ability of PrO_x to provide highly reactive active oxygen, as well as the great ability to produce NO_2, there is a lack of information about the catalytic behavior of pure PrO_x in soot combustion. Praseodymium is usually used as dopant of CeO_2.[14–19] The insertion of dopants perturbs the crystal structure of the catalyst, creating defects that may take form as vacancies or interstitial defects. This may result in more cerium anions in a reduced state (Ce^{3+}), which promotes higher mobility of oxygen ions improving the catalytic activity.[14] Thus, ceria-praseodymia mixed oxides currently have one of the best performances in soot combustion among other ceria-based catalysts.[6,15,18,20,21]

With the above-mentioned background, the catalytic performance in soot combustion of pure praseodymia was analysed in the present work. Moreover, to improve the soot-catalyst contact, three-dimensional ordered macroporous (3DOM) praseodymia catalysts, both pure and doped with copper, have been synthetized, and their catalytic behavior has been studied in the soot combustion in comparison with unstructured catalysts.

Experimental

Catalysts preparation

PrO_x and CuO/PrO_x catalysts have been prepared with uncontrolled (Ref) and three dimensionally ordered macroporous (3DOM) structures. The macroporous catalyst (PrO_x-3DOM) was synthesized by infiltration of the praseodymium precursor in a polymethylmethacrylate (PMMA) colloidal crystal template, which is then removed by calcination. A reference catalyst (PrO_x-Ref) was obtained by direct calcination of the precursor. The PMMA colloidal crystals were prepared by polymerization of methylmethacrylate, methacrylic acid and divinylbenzene (100:1:5 volume ratio) in boiling aqueous solution (H_2O/methylmethacrylate volume ratio 4:1). Polymerization was conducted for 75 min using potassium persulfate as polymerization initiator. After cooling, the colloidal crystals of PMMA were formed by centrifugation at 5000 rpm for 60 min and finally impregnated with an ethanolic praseodymia precursor solution. This solution was prepared dissolving $Pr(NO_3)_3{\cdot}6H_2O$ in ethanol (0.476 M) and adding citric acid in stoichiometric proportion to force the precipitation of metal citrates upon solvent evaporation. Afterwards, the solid was calcined at 600 ^{o}C for 6 hours with a heating rate of 1 ^{o}C/min in order to remove the PMMA template. The reference catalyst (PrO_x-Ref) was prepared following the same procedure

View Article Online
DOI: 10.1039/C9CY00170A

but skipping the impregnation step, that is, the dissolution with citric acid and the Pr precursor was directly dried and calcined.

From PrO_x-3DOM and PrO_x-Ref catalysts, CuO/PrO_x catalysts were prepared by means of excess solvent impregnation on PrO_x supports using an ethanolic copper precursor solution, with the appropriate amount of $Cu(NO_3)_2{\cdot}2.5H_2O$ to achieve a copper loading of 2 wt. %. After evaporation of the solvent, the samples were dried at 80 ^oC overnight and calcined at 500 ^oC for 2 hours, with a heating rate of 5 ^oC/min.

Catalysts characterization

The morphology of the samples was analyzed by Field Emission Scanning Electron Microscope (FESEM) using a Merlin VP Compact microscope from Zeiss, working at very low voltages (from 0.02 kV to 30 kV) to minimize charging effects. The textural characterization of catalysts was carried out by N_2 adsorption at -196 ºC (Autosorb-6, Quantachrome), mercury porosimetry (Poremaster 60 GT, Quantachrome) and helium density (MicroUltrapyc 1200e, Quantachrome). To obtain the N_2 adsorption-desorption isotherms and mercury intrusion profiles, the catalysts were previously outgassed under vacuum at 150 ^oC for 2 h and 50 ^oC for 12 hours, respectively.

The surface chemistry was analyzed by X-ray photoelectron spectroscopy (XPS) in a K-ALPHA Thermo Scientific device, using Al-Kα radiation (1486.6 eV). The X-ray spot was focussed on the catalysts with a diameter of 400 µm, at 3 mA × 12 kV. The binding energy scale was adjusted by setting the C1s transition at 284.6 eV.

Temperature programmed reduction experiments were carried out with H_2 (H_2-TPR) in a thermobalance (Mettler Toledo; TGA/SDTA851) coupled to a mass spectrometer (Pfeiffer Vacuum; Thermostar GSD301T). The catalysts (20 mg) were heated in 5% H_2/Ar (40 ml/min) at 10 ^oC/min from room temperature until 900 ^oC. Temperature Programmed Desorption experiments (Ar-TPD) were carried out in similar conditions but using an Ar flow.

The composition of the catalysts was determined by X-ray microfluorescence in an Obis Micro-XRF Analyzer from EDAX. Areas of 300 µm in diameter were analyzed and three different spots were measured and averaged to obtain the composition of each catalyst.

The crystal structure was analyzed by X-ray diffraction in a Rigaku Miniflex II diffratrometer. The diffractograms were recorded in a range of 2θ from 10^o to 90^o, with a step of 0.025^o. The wavelength used was λ = 0.155418 nm corresponding to the CuK_α radiation. The average crystal size (D) was determined using the Scherrer[22,23] and Williamson-Hall[24] equations. The estimation of crystal size of doped oxides presents some problems, because the introduction of foreign cations within the metal oxide lattice deforms the structure and affects the

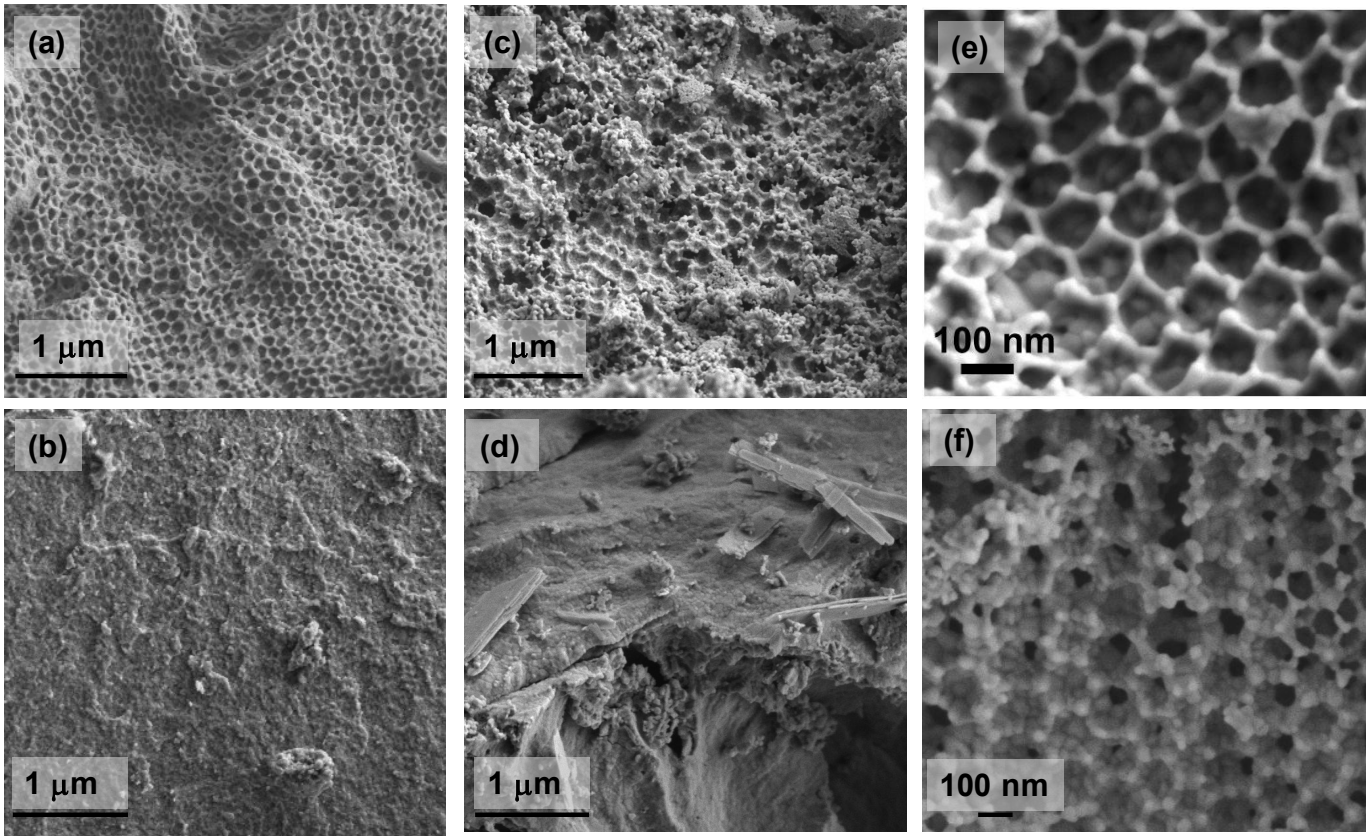

Fig. 1. FESEM images of the (a,e) PrOx-3DOM, (b) PrOx-Ref catalysts, (c,f) CuO/PrOx-3DOM and (d) CuO/PrOx-Ref

peak broadening, and the insertion of copper cations into the metal oxide lattice cannot be ruled out in advance. The Williamson–Hall's equation separates the effects of size and strain in the crystals and is more convenient for the estimation of crystal size of mixed oxides.

Catalytic tests

Catalytic experiments at programmed temperature (25-700 ^{o}C at 10 ^{o}C/min) were carried out in a fixed-bed tubular quartz reactor using a mixture of 20 mg of carbon black (Printex U), 80 mg of catalyst and 300 mg SiC; prepared with a spatula in the so-called loose-contact mode in order to obtain results with practical meaning. Two gas mixtures were used (500 ml/min; GHSV = 30000 h^{-1}): 5% O_2/N_2 and 500 ppm NO/5% O_2/N_2. The composition of the exhaust gases was controlled by specific NDIR-UV gas analysers for CO, CO_2, NO, NO_2 and O_2 (Fisher–Rosemount, models BINOS 100, 1001 and 1004).

Results and discussion

Textural characterization

Representative FESEM images of PrO_x-3DOM and PrO_x-Ref catalysts are shown in Fig. 1. Significant morphological differences were observed between the catalysts. PrO_x-3DOM catalyst exhibits a high-quality three-dimensional structure formed by an ordered network of macropores with a diameter of the order of 80 nm (Fig. 1a and e), whereas the PrO_x-Ref sample presents a closed and compact structure (Fig. 1b). Compared to the average size of PMMA microspheres (ca. 200 nm), the macropore sizes of this 3DOM PrO_x decreased due to the shrinking of PMMA microspheres during the calcination process. After the deposition of CuO on the PrO_x surface, a more closed and not clean 3DOM structure is observed in CuO/PrO_x-3DOM sample (Fig. 1c and f), whereas laminar particles are observed on the surface of CuO/PrOx-Ref.

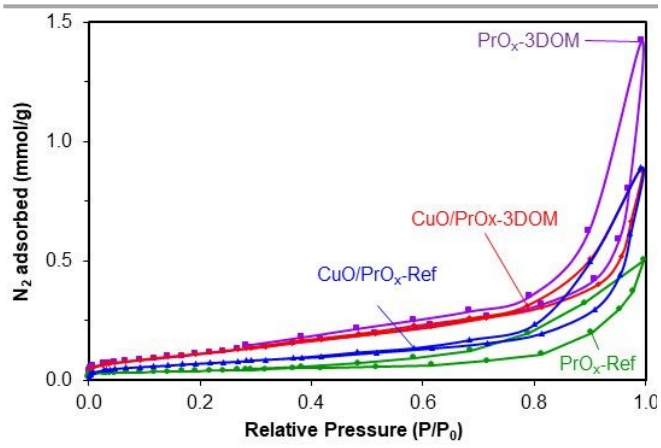

Fig. 2. N_2 adsorption-desorption isotherms at -196 ^{o}C of the catalysts

These morphological differences strongly affect the porosity of the catalysts, as was observed by N_2 adsorption-desorption, mercury intrusion porosimetry and He density measurements. Fig. 2 and 3 show the N_2 adsorption-desorption isotherms and the pore size distributions determined by Hg porosimetry, respectively. The quantitative data obtained by these techniques are collected in Table 1.

Table 1. Results of the catalysts characterization by N_2 adsorption, He density, XRF and XRD.

Catalyst	S_{BET} (m^2g^{-1})	ρ_{He} (gcm^{-3})	Cu (%)	D_S (nm)	D_{WH} (nm)	a (nm)
PrO_x-Ref	3	6.3	-	26	29	0.5459
PrO_x-3DOM	10	6.6	-	26	30	0.5465
CuO/PrO_x-Ref	6	6.9	2.5	25	28	0.5468
CuO/PrO_x-3DOM	9	6.9	3.3	29	31	0.5462

S_{BET}: BET surface area, ρ_{He}: He density, D_x: Fluorite crystallite size determined by Scherrer (S) or Williamson-Hall (WH) equations, a: Fluorite Lattice constant.

All catalysts exhibit a type II isotherm, according with de IUPAC classification, characteristics of non-porous or macroporous adsorbent. The low N_2 adsorption at low relative pressures denotes a low microporosity, whereas the certain adsorption and the hysteresis loop at intermediate or high relative pressures suggest the existence of both mesopores and macropores. Note that the stronger and faster adsorption at high relative pressures of sample PrO_x-3DOM denotes the presence of higher volume of macropores, as is corroborated by SEM. In turn, the deposition of copper oxide particles on the PrO_x supports provokes a different effect on the porosity depending of the sample and the porosity range. In both cases, PrO_x-3DOM and PrO_x-Ref, the loop appears at 0.3-0.4 relative pressure, indicating the presence of certain narrow mesoporosity. After the deposition of CuO, the loop begins at higher relative pressures (0.6-0.7) at the same time that the adsorption at intermediate P/P_0 decreases, which indicates a mesoporosity blockage by the deposition of CuO nanoparticles. Regarding the wider porosity, the CuO particle deposition induces a strong decrease in the N_2 uptake at high P/P_0 in PrO_x-3DOM sample, suggesting the presence of a lower amount of macropores. This seems to indicate that, in the case of the 3DOM sample, the CuO particles are distributed throughout all the porosity range of the praseodymia support blocking part of the created 3D ordered macroporosity. Conversely, an increase of such N_2 uptake occurs in the PrO_x-Ref after impregnation with copper. The porosity created in PrO_x catalysts could remain closed due to the accumulation of carbonates and/or bicarbonates. Part of these carbonates/bicarbonates are removed after copper impregnation due to the slightly acid pH (pH = 5.5) of the copper nitrate solution used for impregnation, which would favor the release of CO_2 chemisorbed on the solid opening of the porosity (i.e. in the case of PrO_x-Ref). In CuO/PrO_x-3DOM, the porosity opening by the removal of carbonates/bicarbonates occurs simultaneously with the porosity blockage by the deposition of CuO particles, being the later effect more significant.

The BET surface areas (Table 1) are consistent with the above described porosity opening and blockage. The S_{BET} was 3 and 6 m^2/g for PrO_x-Ref and CuO/PrO_x-Ref, respectively, that

is, part of the closed porosity by carbonates/bicarbonates is opened upon impregnation. Conversely, the S_{BET} was 10 and 9 m^2/g for PrO_x-3DOM and CuO/PrO_x-3DOM, respectively, that is, part of the porosity of PrO_x-3DOM is blocked by the copper species loaded to obtain the CuO-catalyst.

These observations were corroborated by Hg porosimetry and He density measurements. As expected (Figure 3), both PrOx-3DOM catalysts present a well-defined peak for pore radius around 40 nm. The amount of these pores decreases after Cu-impregnation, due to blockage by the deposition of CuO particles in the porosity. This peak is not observed in the case of reference catalysts, in which there is a peak around 700 nm ascribed to interparticular spaces. Regarding the He data (Table 1), the expected He density for bulk Pr_6O_{11} is 6.9 g/cm^3.[25] The density values of PrO_x-Ref and PrO_x-3DOM are lower than the expected one, denoting the existence of closed porosity, which is not accessible neither for He in density measurements nor for N_2 during adsorption-desorption at -196 ^oC. This difference in densities is greater in the case of PrO_x-Ref, which indicates the existence of greater closed porosity and, apparently, a greater amount of carbonates/bicarbonates in this case. The increase of the density up to the theoretical value after copper impregnation confirms that the closed porosity gets open due to the elimination of carbonates/bicarbonates.

Crystalline structure (XRD)

The crystalline structure of the catalysts was characterized by XRD. Fig. 4 shows the X-Ray diffractograms, and Table 1 compiles several parameters determined from these diffractograms. The diffractograms reveal the stabilization of fluorite-structured cubic Pr_6O_{11} in all catalysts (JCPDS PDF # 42-1121). In turn, the lattice parameters are very similar and are consistent with the value reported in the JCPDS database (0.5467 nm)[26] suggesting that PMMA template does not affect the primary crystals of Pr_6O_{11} and that copper is not introduced into the praseodymia lattice. As consequence, upon copper loading, broad and not very well-defined peaks of CuO are observed at characteristic 2θ angles (35.5^o and 38.8^o),

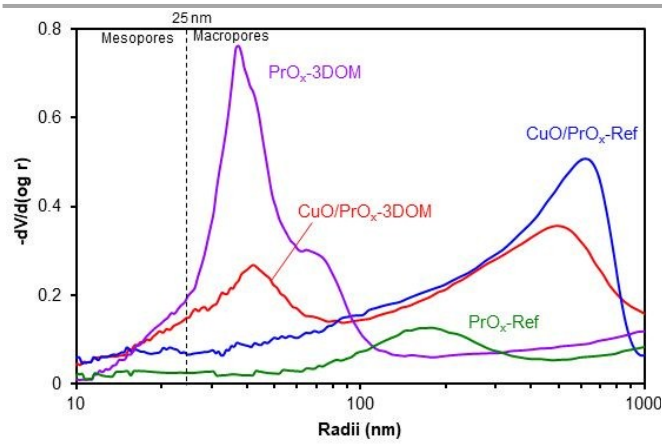

Fig. 3. Pore size distributions determined by mercury intrusion porosimetry

Table 2. Surface characterization by XPS.

Catalyst	Pr^{3+} (%)[1]	Pr^{3+} (%)[2]	% $C_{carbonates}$[3]	O_{ads}/O_{latt}
PrO_x-Ref	33.5	33.4	22.5	1.86
PrO_x-3DOM	52.6	50.4	20.3	2.01
CuO/PrO_x-Ref	-	76.7	17.2	2.21
CuO/PrO_x-3DOM	-	85.6	15.9	2.57

[1] % of Pr^{3+} determined by Borchert et al equation, [2] % of Pr^{3+} determined by the proposed equation 1, [3]% of Peak at 289.2 eV

suggesting a high dispersion of copper oxide on the catalysts surface. The CuO particle size, obtained by applying the Scherrer's equation, was 15 nm and 21 for CuO/PrOx-3DOM and CuO/PrOx-Ref, respectively. Surface accumulation of copper favors the blocking of the porosity observed by N_2-adsorption.

The crystal sizes obtained for the Pr_6O_{11} phase are quite similar in all samples (28-31 nm) suggesting again that the presence of the PMMA template does not affect the primary crystals. Minor differences are observed between values obtained with the Scherrer's and Williamson Hall's equations, suggesting that, in this case, crystal strain has a minor contribution to XRD peaks broadening, ruling out the incorporation of copper cations into the support lattice.

Surface chemistry (XPS)

The surface chemistry of samples was analysed by XPS. Shown in Fig. 5 are the O_{1s} and Pr_{3d} spectra of PrO_x-catalysts. Two sets of signals are observed in Pr3d region, one centred at BE = 924-937 eV assignable to Pr $3d_{3/2}$ and the other centred at BE = 943-960 eV assignable to Pr $3d_{5/2}$. These regions could be decomposed into seven peaks organized, according to the literature, into 3 spin-orbit split doublets: a-b, a'-b' and a''-b''.[27] The $3d_{3/2}$ sublevel presents an additional peak "t", which can be explained by a multiplet effect.[27] The direct peak association and quantification of Pr^{3+} and Pr^{4+} species is not possible. Doublets a-b and a'-b' are presents in both pure Pr^{3+}

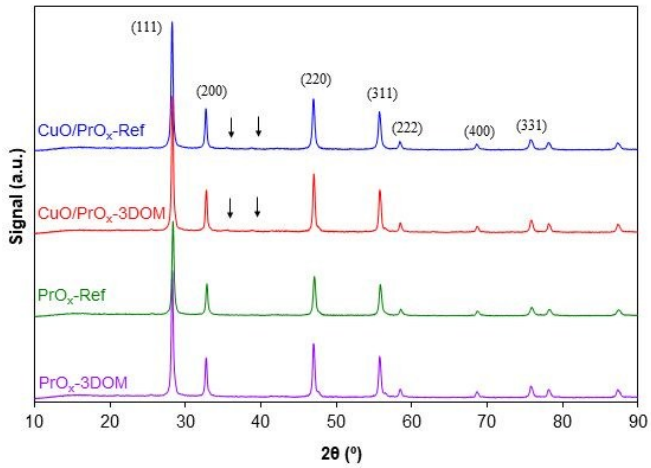

Fig. 4. X-Ray diffractograms of the catalysts. Indexed peaks belong to the Pr6O11 phase and arrows to CuO.

(Pr_2O_3) and Pr^{4+} (PrO_2) oxides. However, a'' and b'' peaks are exclusively observed in PrO_2 and thus, ascribed to Pr^{4+}.[27–29] Borchert *et al.* have observed that a'' decreases after reduction with CH_4 whereas a' and a peaks remain almost constant. At this way, the Pr^{3+} amount could be estimated considering the peak area ratio of a''/a' by the empirically equation of Borchert *et al*.[27] This equation could be used in the case of PrO_x catalysts (PrO_x-Ref and PrO_x-3DOM) but not for CuO/PrO_x ones in which Cu_{2p} signals appear at around 930-937 eV and consequently, overlaps with a' peak. Nevertheless, this equation could be reformulated and referred to the a''/a peak area ratio, and thus, the Pr^{3+} amount in CuO/PrO_x catalysts could be estimated by the following equation:

$$Pr^{3+}(\%) = 100 \cdot \left(1 - \frac{1}{0.62} \cdot \frac{a''}{a}\right) \quad (1)$$

Results are collected in Table 2. Pr^{3+} (%) values obtained using the proposed equation are very closed to the data obtained with Borchert *et al.* one (error lower than 4 %), verifying the validity of the proposed equation to estimate the oxidation state of the praseodymium ions in Cu/PrO_x catalysts. Moreover, a clearly decrease of *a''* and *b''* peak area (peaks ascribed to Pr^{4+}) is observed in the trend PrO_x-Ref > PrO_x-3DOM > CuO/PrO_x-Ref > CuO/PrO_x-3DOM. These peaks practically disappear in the case of Cu/PrO_x-3DOM denoting an enrichment of low oxidation state praseodymium ions on the surface, which corroborate the % Pr values obtained with the proposed equation. The theoretical average valence of Pr in Pr_6O_{11} is 3.66. Therefore, the spectral region of Pr must be composed by a mixture of 66.7% Pr^{4+} and 33.3% Pr^{3+}.[30] The % of Pr^{3+} agrees with the theoretical value in PrO_x-Ref catalyst (Table 2). However, a higher percentage is obtained in PrO_x-3DOM catalyst, denoting a surface oxygen deficiency in this case. This higher surface oxygen vacancies in 3DOM samples could be ascribed to the presence of PMMA template. PMMA template leads to the creation of a higher population of oxygen defects on the praseodymium oxide than direct calcination of the metal precursors because of, during calcination, an O_2-poor environment is expected due to oxygen consumption by PMMA combustion and external O_2 diffusion restrictions inside the solid.[31] This oxidation of praseodymium precursors in an O_2-poor environment could improve the creation of oxygen vacancies on the metal oxide, as was pointed out in a previous study.[32] The % of Pr^{3+} increases with the presence of copper and, again, this percentage is higher in the case of the 3DOM sample due to the effect of PMMA combustion. It is well known that the addition of copper to ceria enhances the redox behaviour, the ceria reducibility and the oxygen storage capacity and the thermal stability of ceria.[33] Similar results could be expected in CuO/PrO_x and consequently, the high surface enrichment in Pr^{3+} observed by XPS in CuO/PrO_x catalysts might be due to the surface enrichment in Pr^{3+} ions and/or to the self-reduction of the sample under ultra-high vacuum (ca. 10^{-9} mbar) in the XPS chamber[34,35] due to the improved reducibility of praseodymia in the presence of copper.

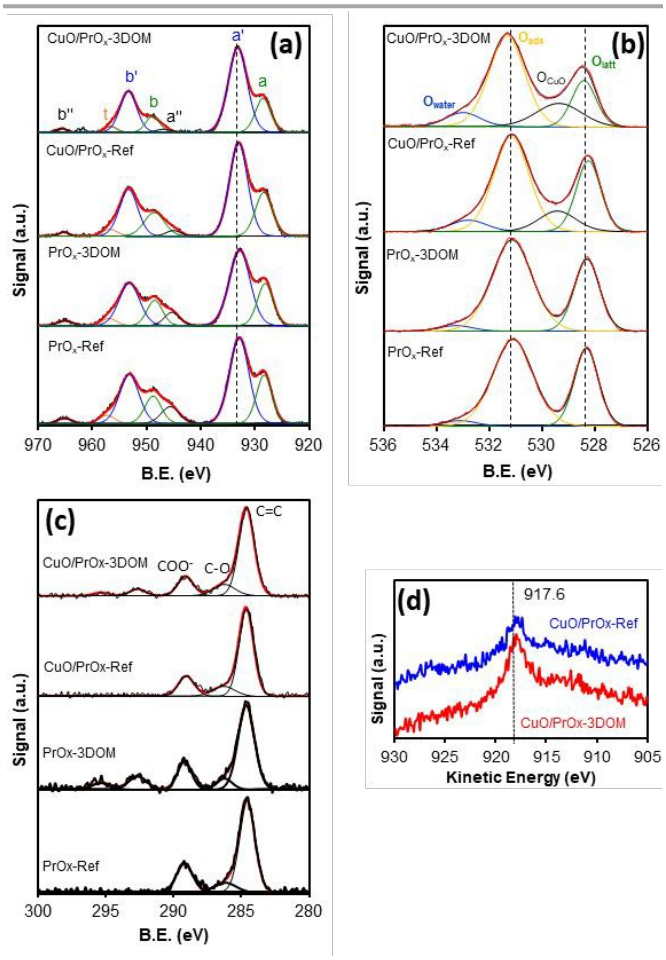

Fig. 5. XPS characterization of the catalysts surface. (a) Pr 3d, (b) O1s, (c) C 1s regions and (d) Cu LMM Auger range.

These conclusions were corroborated analysing the O_{1s} region. This region could be decomposed into three components at BE = 528.3, 531.1 and 533.1 eV, which were attributable to the surface lattice oxygen (O_{latt}), the adsorbed oxygen species (O_{ads}, e.g. O^-, O_2^{2-} or O_2^-) and adsorbed molecular water, respectively. An additional peak at 529.3 is observed in Cu/PrO_x catalysts which was ascribed to CuO. The Cu LMM Auger transition (Fig. 5d) is centered at about 917.6 eV, which also supports the presence of CuO.

The O_{ads} species are usually present at the oxygen vacancies. A large amount of O_{ads} species implies a higher oxygen vacancy density. The surface O_{ads}/O_{latt} molar ratios of PrO_x catalysts are collected in Table 2. PrO_x-3DOM sample has higher O_{ads}/O_{latt} ratio than the reference catalyst, which corroborates the existence of a greater number of superficial oxygen vacancies. In addition, it is observed that, after copper deposition, this content increases, mainly in CuO/PrO_x-3DOM sample, according with the trend observed in % of Pr^{3+}. It is well accepted that the presence of oxygen vacancies is favourable for the improvement in reducibility. Therefore, Cu-catalysts are expected to exhibit better reducibility, as substantiated by the H_2-TPR results shown in below.

The presence of carbonates/bicarbonates was also pointed out by XPS (Table 2 and Fig. 5c). As it was described previously, the amount of carbonates/bicarbonates is higher in the case of Ref-samples regarding the 3DOM ones (22.5 and 17.2 vs 20.3 and 15.9, respectively). Note that a decrease of the surface

View Article Online
DOI: 10.1039/C9CY00130A

carbonates/bicarbonates concentration is observed after copper impregnation, which corroborates the closed porosity by carbonate/bicarbonate hypothesis described above.

Temperature Programmed Reduction (H_2-TPR) and Decomposition (Ar-TPD)

The reducibility of the catalysts was studied by H_2-TPR experiments and m/z 18 signal profiles, which belongs to H_2O, are depicted in Fig. 6. Note that changes in m/z 2 signal of H_2 are very small, and the reduction events can be hardly studied following this signal. That is why the m/z 18 has been used.

The m/z 18 signal of copper-free PrOx catalysts present two main peaks (Fig. 6) located at 300 °C and between 400 and 600 °C. The first one is attributed to the decomposition of praseodymium bicarbonates, previously described, observing a greater quantity of bicarbonates in the PrO_x-Ref sample compared to 3DOM. The second peak is attributed to the reduction of Pr_6O_{11} to Pr_2O_3. As was described in literature,[36] this reduction occurs in two steps with the appearance of two fused peaks: $PrO_{1.83} \xrightarrow{480\,^oC} PrO_{1.61} \xrightarrow{540\,^oC} PrO_{1.5}$.[36] This peak is similar in intensity and position in both catalysts (Ref and 3DOM), which denotes a similar reducibility. However, it should be noted that the intensity of the peak at 480 °C decreases in the case of the 3DOM catalyst due to the greater surface reduction observed by XPS. In copper-containing samples, a peak at 290 °C is observed, attributed to the reduction of CuO in intimate contact with praseodymia, overlapped with a long tail up to 400-500 °C due to the reduction of copper-catalyzed praseodymia, ie the reduction of Pr^{4+} cations that are in close contact with copper species. The two typical CuO reduction peaks are not observed in Fig. 6, and instead, a main peak at 290 °C appears ascribed to copper-catalyzed praseodymia reduction, denoting a good copper oxide-praseodimium oxide interaction in both cases.

To corroborates the peak assignation to bicarbonates, temperature programmed decomposition was performed in Ar atmosphere (Fig. 7). Note that m/z 18 signal peak at 300 °C is also obtained in non-reducing atmosphere and is accompanied by a release of CO_2, according with bicarbonates decomposition. This m/z 18 peak is more intense in PrO_x-Ref regarding PrO_x-3DOM catalysts and practically disappears after the Cu impregnation due to the removal of carbonates/bicarbonates by the acidic impregnation solution, which corroborates previous observations.

Catalytic combustion of soot with O_2

Soot combustion experiments were performed under 5%O_2/N_2, and the CO_x evolution profiles are shown in Fig. 8. All catalysts accelerate the combustion of soot with regard to the unanalyzed reaction (Fig. 8), and the catalytic activity depends on the catalyst composition, morphology and active surface. PrO_x-Ref is the least active catalyst both in the presence and absence of NO_x while PrO_x-3DOM is the most active. This denotes that the 3DOM structure improves the catalytic activity. The presence of copper improves the catalytic activity in the case of PrO_x-Ref catalyst, while in the 3DOM catalyst this improvement is not observed but, even, a loss of activity is obtained regarding copper-free 3DOM catalyst; a fact that occurs both in presence and in absence of NO_x. There are two soot combustion mechanisms to consider, the so-called "active oxygen" mechanism and the so-called "assisted by NO_2" one. In the former (in the absence of NO_x), combustion takes place by oxygen species radicals of praseodymia (active oxygen), partially reducing the Pr^{4+} cations to Pr^{3+}, while oxygen vacancies created in the catalyst play a bridge role in the capture or transfer of electrons and convert molecular oxygen into new active oxygen species to interact again with the soot in contact with the interface. Thus, there are two crucial stages in this mechanism: the production of "active oxygen" (affected by the catalyst reducibility) and its transfer from the solid catalyst to soot particles (limited by the contact points available and consequently, affected by the catalyst surface). Both aspects are enhanced in the PrO_x-3DOM catalyst: greater is the number of O_{ads} and oxygen vacancies (observed by XPS) and the catalyst-carbon contact due to the macroporous structure. The presence of copper has several effects: i) improvement of the reducibility of praseodymia (Fig. 6) and ii) modification of textural properties (Fig. 2 and Table 1). In CuO/PrO_x-Ref, both the surface and, therefore, the contact with the carbon (due to the elimination of carbonates/bicarbonates), as well as the reducibility due to the presence of copper, are improved with respect to PrO_x-Ref and consequently, the activity is improved regarding copper-free catalyst. However, the addition of copper to the 3DOM catalyst produces a macroporosity blockage, and hence, despite the improvement of the reducibility and production of

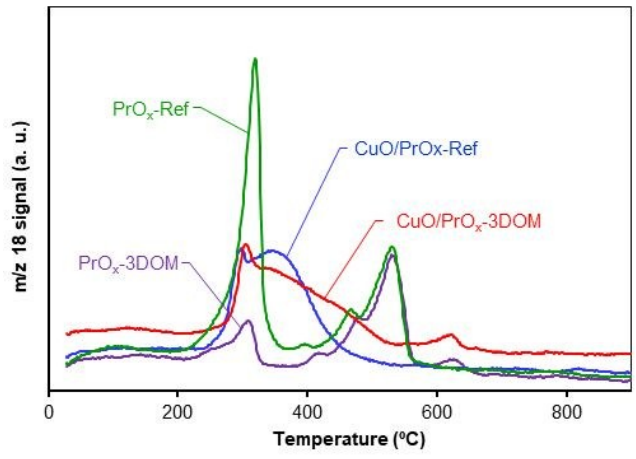

Fig. 6. H_2-TPR characterization of the catalysts.

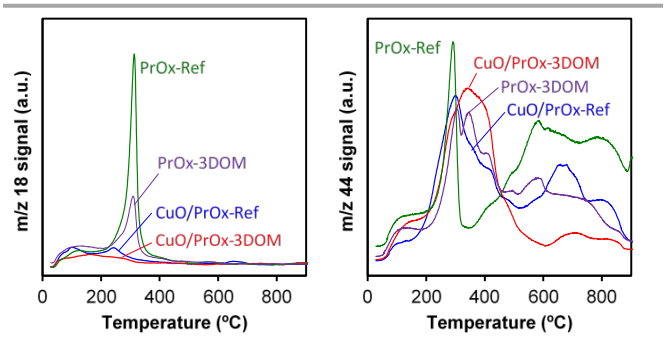

Fig. 7. Ar-TPD characterization of the catalysts.

active oxygen, the catalyst-carbon contact obtained with the ordered macroporous structure is reduced, reducing the activity of CuO/PrO_x-3DOM up to the degree of CuO/PrO_x-Ref. According to these results, the catalytic activity for soot combustion in 5%O_2/N_2 follows the trend PrO_x-3DOM > CuO/PrO_x-3DOM ~ CuO/PrO_x-Ref >> PrO_x-Ref. The trend in O_{ads} and reducibility is CuO/PrO_x-3DOM > CuO/PrO_x-Ref > PrO_x-3DOM > PrO_x-Ref while in surface is PrO_x-3DOM > CuO/PrO_x-3DOM > CuO/PrO_x-Ref > PrO_x-Ref manifesting that the limiting factor in soot combustion is the soot-catalyst contact and the transfer of active oxygen from catalyst to soot particles despite the production of active oxygen.

The effect of NO_x in the catalytic combustion of soot was studied, and two types of experiments were performed using a gas mixture with NO + O_2. The catalytic combustion of soot was studied with soot + catalyst mixtures and the catalytic oxidation of NO to NO_2 was studied in experiments performed only with the catalysts (without soot).

In presence of NO, the main NO_x present in the residual gas of diesel engines, it should be further considered the "NO_2-assisted mechanism". If temperature is high enough (above 300 °C) PrO_x is able to catalyze the oxidation of NO to NO_2 which also participates efficiently in the oxidation of soot. In this mechanism two factor must be taken into account: i) the produced NO_2 is much more oxidising than O_2 and NO, and could directly react with soot solving the problem of poor contact between soot and catalyst and ii) NO_2 interacts with the catalyst to create more active oxygen,[37] this is, NO_2 is a strong oxidising agent and it is postulated that NO_2 is able to transfer its oxygen to the catalyst surface.[9] The desorption of stored oxygen generated by the NO_2-PrO_x reaction may also produce active oxygen species which can be transferred to the soot surface to accelerate the oxidation, as described for CeO_2.[38] NO_2 profiles in catalytic experiments are depicted in Fig. 9a. In the absence of soot, the NO_2 profiles increase with temperature until a maximum where thermodynamic equilibrium is achieved, and above that temperature the NO_2 profiles decrease following thermodynamics. Note that praseodymia presents an important ability for the NO_2 production,[13] greater than similar ceria catalysts (40 % and 10 % at 400 ºC for PrO_x-3DOM and CeO_2-3DOM, respectively).

In this sense, it is observed that all catalysts accelerate the combustion of soot because of NO_2 also participates in the soot oxidation (Fig. 8). However, despite all catalysts have the same capacity to oxidize NO to NO_2 (Fig. 9a), a different catalytic improvement regarding NOx-free experiences is obtained (Fig. 10). NO_x decreases the T50% temperature for all catalysts, but the effect is much more relevant for PrO_x-3DOM, CuO/PrO_x -Ref and CuO/PrO_x-3DOM than for PrO_x-Ref. Note that this improvement depends again on the surface area and reducibility of the catalyst. This fact indicates that the main pathway is not the direct reaction of NO_2 with soot because of the problem of poor contact between soot and catalyst is not solved but NO_2 reacts with PrO_x surface creating more active oxygen to react and be transfer to soot particles and consequently, this pathway depends on the characteristics of the catalysts. In PrO_x-Ref sample, the few points of contact with the soot limit the transfer of this active oxygen, limiting its potential for improvement in the presence of NO_x (Fig. 10).

To analyze the reaction of NO_2 with soot, the NO_2 profiles in presence of soot were also recorded (Fig. 9b). Most NO_2 produced by copper-free catalysts is consumed during the reaction with soot. However, despite all catalysts have the same ability to produce NO_2 (see profiles in Fig. 9a) in experiments with soot (Fig. 9b) the NO_2 profiles of CuO-containing catalysts show higher NO_2 concentrations than the CuO-free counterparts. This fact cannot be explained on the basis of a lower reaction with soot, because a similar improvement in soot combustion, e.g. for PrO_x-3DOM and CuO/PrO_x-3DOM, is obtained in presence of NO_x. It seems to be more reasonable think that each NO molecule is oxidized several times during the residence time into the catalytic bed. Since copper accelerates the NO oxidation to NO_2, the catalytic oxidation rate of NO to NO_2 is faster than the NO_2 reduction rate by reaction with soot.

Both oxygen vacancies and surface active oxygen play important roles in oxidation reactions.[40] However, H.Wang *et al*.[40] have demonstrated that the contribution of surface oxygen vacancies of ceria to NO oxidation is lower than expected, whereas the lattice and/or active oxygen over ceria played more important roles. At this way, samples with more surface oxygen vacancies and less active oxygen species exhibited lower NO oxidation activity. Consequently, active

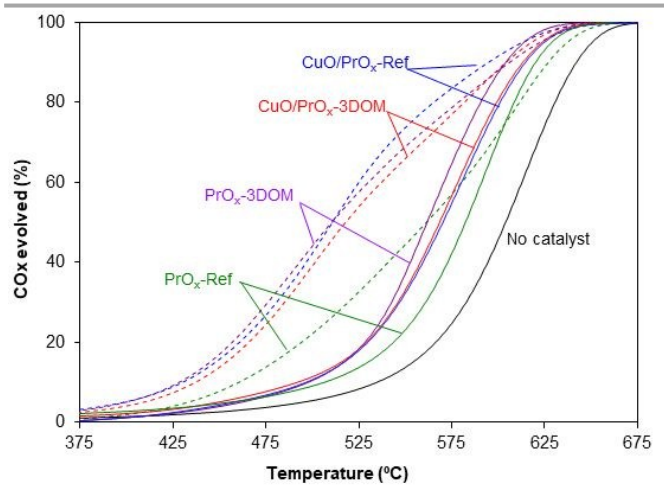

Fig. 8. Soot combustion experiments with 5% O_2 + N_2 (solid lines) and 500 ppm NOx + 5% O_2 + N_2 (dotted lines)

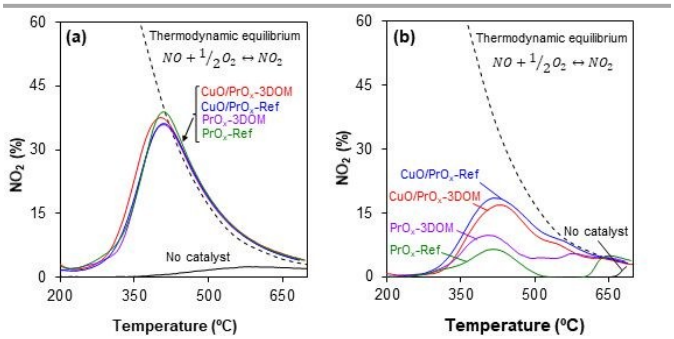

Fig. 9. NO_2 profiles in catalytic experiments performed a) without and b) with soot.

oxygen species (O_x^-) is an important reactivity descriptor for NO oxidation other than surface oxygen vacancies for CeO_2-based catalysts.[40] Despite the different surface oxygen vacancies content of PrO_x catalysts (XPS results), all catalysts have the same capacity to oxidize NO to NO_2 (Figure 9a) in absence of soot, whereas in presence of soot, the ability of copper to accelerates the NO oxidation to NO_2 is, then, observed. This could indicate that in absence of soot the production of NO_2 is limited by the thermodynamics, and only when part of NO_2 reacts with soot, the differences ability to catalyze the oxidation of NO are observed. To corroborate this fact, m/z 32 signal was followed in Ar-TPD tests (Figure S1). The evolution of the O_2 release is very similar for all samples, note only that slightly differences are observed at 300 ºC and 680 ºC. A release of O_2 is observed at 300 ºC for PrO_x-Ref and PrOx-3DOM which is attributed to the decomposition of carbonates/bicarbonates present only in these two samples. At 680 ºC, a release of O_2 is observed for CuO-based samples, but this temperature is higher enough to limit the production of NO_2 by the thermodynamics and, consequently, differences in the NO_2 production are not observed.

It is known that NO is the main nitrogen-containing product of the NO_2-soot reaction,[9] but the NO_x-soot reaction also yields some N_2.[41] To identify the NO_x reduction by soot, the NO_x profiles have been included in Fig. 11. There are not evidences of net NO_x removal from the gas stream in the 200-700 ºC range during the catalytic experiments performed without soot. This means that NO_x chemisorption on the catalysts do not occur. However, in presence of soot, all NO_x profiles obtained show a minimum that must be attributed to NO_x reduction by soot, which occurs together with soot gasification. Similar NO_x reduction is detected for all catalysts (around 10 %) and consequently, a similar interaction of NO_x with soot could be deduced. Summarizing, similar production of NO_2 and reduction of NO_x is detected in all catalysts denoting a similar combustion of soot by direct reaction with NO_2. This would mean that the same improvement of the combustion of soot in presence of NO with regard to O_2 combustion would be expected. However, the improvement in PrO_x-Ref by the NO_x-combustion is lower than expected. This manifests that the direct reaction of NO_2 with soot is not the main pathway in the NO_2-assisted combustion of soot using PrO_x catalysts, but the most significant pathway is the NO_2 interaction with the catalyst to create more active oxygen to be transferred to the soot. The former depends on the NO_2 production and concentration and it is not limited by the soot-catalyst contact points, whereas the latter is strongly influenced by these contact points (active-oxygen mechanism). It is observed that the NO_2-assisted combustion of soot depends on the surface area and catalyst reducibility, and not on the NO_2 production. In summary, it could be concluded that NO_2 mainly reacts with PrO_x surface creating active oxygen that is transferred to soot particles and consequently, the improvement in presence of NO depends on the surface area of support.

Conclusions

A three-dimensionally ordered macroporous (3DOM) PrOx catalyst with improved efficiency for the soot combustion has been prepared. The main phase detected by XRD on this catalyst is Pr_6O_{11}, and the crystalline parameters are equal to those of a counterpart reference catalyst prepared without a defined structure.

The PrO_x-3DOM catalyst has ordered macroporosity with pores of 80 nm in diameter, which favors the carbon-catalyst contact. In addition, the 3DOM catalyst presents higher surface density of active oxygen (O_{ads}). Consequently, the PrO_x-3DOM catalyst combines a good production of active oxygen and an efficient transfer to soot, being highly active catalyst to accelerate soot combustion.

The effect of CuO loading has been studied. The impregnation of copper on a PrO_x support with a conventional structure (CuO/PrO_x-Ref) enhances the production and transfer to soot of active oxygen, improving the activity with respect to CuO-free PrO_x-Ref. However, CuO blocks the porosity of the PrOx-3DOM support, hindering the contact with soot.

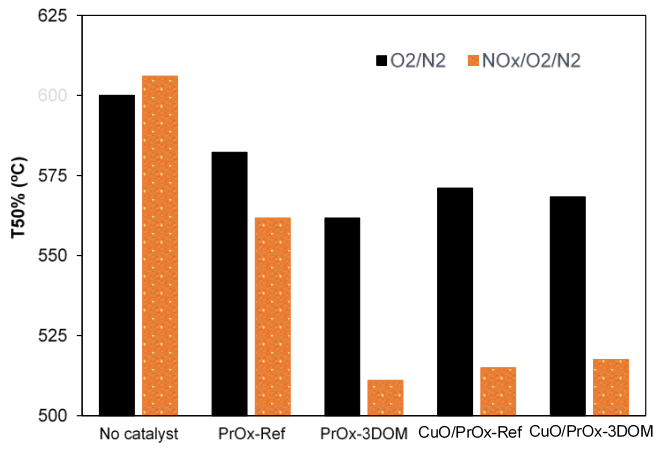

Fig. 10. Temperature for 50% soot combustion in experiments performed with and without NO_x in the gas mixture.

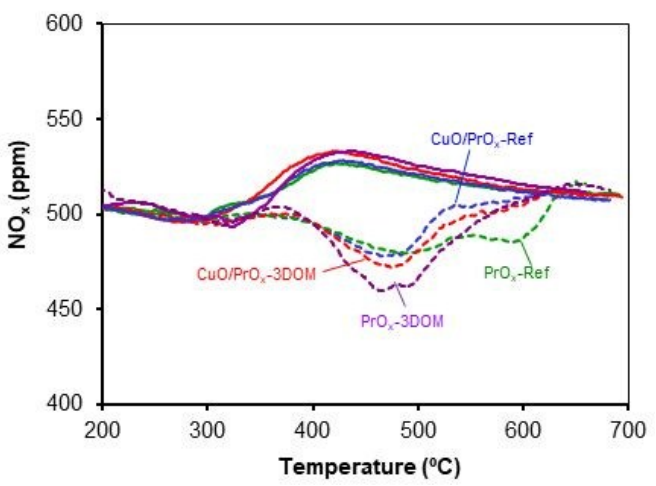

Fig. 11. NO_x profiles in catalytic experiments performed with (dashed line) and without (continuous line) soot.

Soot combustion is accelerated in the presence of NOx due to the production of NO_2 catalysed by PrO_x. This NO_2, once produced, is mostly readsorbed on the surface of the catalysts producing active oxygen that must be transferred to soot. For this reason, the porosity of the catalysts also plays a relevant role during combustion with NO_x/O_2 because affects the transfer of active oxygen produced by NO_2 to soot, and the 3DOM structure improves such transfer.

Conflicts of interest

There are no conflicts to declare.

Acknowledgements

The authors thank the financial support of the Spanish Ministry of Economy and Competitiveness (Project CTQ2015-67597-C2-2-R and grant FJCI-2015-23769), the Spanish Ministry of Education, Culture and Sports (grant FPU14/01178) and the UE (FEDER funding).

Notes and references

1 N. Hickey, I. Boscarato and J. Kaspar, in *Current Environmental Issues and Challenges*, eds. G. Cao and R. Orrù, Springer, Netherlands, 2014, pp. 15–43.
2 M. V. Twigg, *Catal. Today*, 2011, **163**, 33–41.
3 N. Russo, D. Fino, G. Saracco and V. Specchia, *J. Catal.*, 2005, **229**, 459–469.
4 US 2002/0083699, 2002.
5 C. Xu and X. Qu, *NPG Asia Mater.*, 2014, **6**, e90.
6 A. Bueno-López, *Appl. Catal. B Environ.*, 2014, **146**, 1–11.
7 Q. Liang, X. Wu, D. Weng and Z. Lu, *Catal. Commun.*, 2008, **9**, 202–206.
8 I. P. Kandylas and G. C. Koltsakis, *Ind. Eng. Chem. Res.*, 2002, **41**, 2115–2123.
9 A. Setiabudi, J. Chen, G. Mul, M. Makkee and J. A. Moulijn, *Appl. Catal. B Environ.*, 2004, **51**, 9–19.
10 G. Zhang, Z. Zhao, J. Xu, J. Zheng, J. Liu, G. Jiang, A. Duan and H. He, *Appl. Catal. B Environ.*, 2011, **107**, 302–315.
11 Y. Wei, Z. Zhao, X. Yu, B. Jin, J. Liu, C. Xu, A. Duan, G. Jiang and S. Ma, *Catal. Sci. Technol.*, 2013, **3**, 2958–2970.
12 N. Feng, C. Chen, J. Meng, G. Liu, F. Fang, J. Ding, L. Wang, H. Wan and G. Guan, *Catal. Sci. Technol.*, 2017, **7**, 2204–2212.
13 N. Guillén-Hurtado, F. E. López-Suárez, A. Bueno-López and A. García-García, *React. Kinet. Mech. Catal.*, 2014, **111**, 167–182.
14 T. Andana, M. Piumetti, S. Bensaid, N. Russo, D. Fino and R. Pirone, *Nanoscale Res. Lett.*, 2016, **11**, 278–286.
15 N. Guillén-Hurtado, A. García-García and A. Bueno-López, *Appl. Catal. B Environ.*, 2015, **174–175**, 60–66.
16 A. D. Logan and M. Shelef, *J. Mater. Res.*, 1994, **9**, 468.
17 A. Torkkeli, *VTT Publ.*, 2003, **63**, 3–194.
18 T. Andana, M. Piumetti, S. Bensaid, N. Russo, D. Fino and R. Pirone, *Appl. Catal. B Environ.*, 2016, **197**, 125–137.
19 M. Florea, G. Postole, F. Matei-Rutkovska, A. Urda, F. Neaţu, L. Massin and P. Gelin, *Catal. Sci. Technol.*, 2018, **8**, 1333–1348.
20 D. Fino and V. Specchia, *Chem. Eng. Sci.*, 2004, **59**, 4825–4831.
21 E. Cauda, D. Fino, G. Saracco and V. Specchia, *Top. Catal.*, 2007, **45**, 125–129.
22 A. W. Burton, K. Ong, T. Rea and I. Y. Chan, *Microporous Mesoporous Mater.*, 2009, **117**, 75–90.
23 P. Scherrer, *Göttinger Nachrichten Math. Phys*, 1918, **2**, 98–100.
24 G. K. Williamson and W. H. Hall, *Acta Metall.*, 1953, **1**, 22–31.
25 P. Villars and K. Cenzual, Eds., .
26 Y. Zhang, K. Han, X. Yin, Z. Fang, Z. Xu and W. Zhu, *J. Cryst. Growth*, 2009, **311**, 3883–3888.
27 H. Borchert, Y. V. Frolova, V. V. Kaichev, I. P. Prosvirin, G. M. Alikina, A. I. Lukashevich, V. I. Zaikovskii, E. M. Moroz, S. N. Trukhan, V. P. Ivanov, E. A. Paukshtis, V. I. Bukhtiyarov and V. A. Sadykov, *J. Phys. Chem. B*, 2005, **109**, 5728–5738.
28 A. Bianconi, A. Kotani, O. Okada, R. Giorgi, A. Gargano, A. Marcelli and T. Miyahara, *Phys. Rev. B*, 1988, **38**, 3433–3437.
29 H. Ogasawara, A. Kotani, R. Potze, G. A. Sawatzky and B. T. Thole, *Phys. Rev. B*, 1991, **44**, 5465–5469.
30 Y. Wang, Z. Peng, Q. Wang and X. Fu, *Sci. Rep.*, 2016, **7**, 41994–42006.
31 A. Davó-Quiñonero, J. González-Mira, D. Lozano-Castelló and A. Bueno-López, *Catal. Letters*, 2018, **148**, 258–266.
32 A. Davó-Quiñonero, J. González-Mira, I. Such-Basañez, J. Juan-Juan, D. Lozano-Castelló and A. Bueno-López, *Catalysts*, 2017, **7**, 67.
33 C. G. Maclel, T. D. F. Silva, M. I. Hirooka, M. N. Belgacem and J. M. Assaf, *Fuel*, 2012, **97**, 245–252.
34 F. Zhang, P. Wang, J. Koberstein, S. Khalid and S. W. Chan, *Surf. Sci.*, 2004, **563**, 74–82.
35 E. Poggio, M. Jobbágy, M. Moreno, M. Laborde, F. Mariño and G. Baronetti, *Int. J. Hydrogen Energy*, 2011, **36**, 15899–15905.
36 M. F. Luo, Z. L. Yan and L. Y. Jin, *J. Mol. Catal. A Chem.*, 2006, **260**, 157–162.
37 I. Atribak, F. E. López-Suárez, A. Bueno-López and A. García-García, *Catal. Today*, 2011, **176**, 404–408.
38 S. Liu, X. Wu, Y. Lin, M. Li and D. Weng, *Chinese J. Catal.*, 2014, **35**, 407–415.
39 V. Alcalde-Santiago, A. Davó-Quiñonero, D. Lozano-Castelló and A. Bueno-López, *Appl. Catal. B Environ.*, 2018, **234**, 187–197.
40 H. Wang, S. Luo, M. Zhang, W. Liu, X. Wu and S. Liu, *J. Catal.*, 2018, **368**, 365–378.
41 I. Atribak, A. Bueno-López and A. García-García, *J. Catal.*, 2008, **259**, 123–132.